Supplementary Materials for "Central posterior envelopes for Bayesian functional principal component analysis"

Joanna Boland, Donatello Telesca, Catherine Sugar, Michele Guindani, Shafali Jeste, Abigail Dickinson, Charlotte DiStefano, and Damla Şentürk

Appendix A. Posterior Distributions for BFPCA

Using Gaussian priors for the mean coefficients $\boldsymbol{\beta}$ and factor loadings $\boldsymbol{\lambda}_\ell$, noninformative prior for the error variance σ^2_ϵ (proportional to a constant c), gamma prior for the variance of the mean coefficients σ^2_β and a modified multiplicative gamma process shrinkage (MMGPS) prior for the variance components of the factor loading matrix $\sigma^2_{\lambda_{r\ell}}$, the model can be given in matrix form as:

$$\boldsymbol{Y}_i = \boldsymbol{f}_i + \boldsymbol{\epsilon}_i = B(\boldsymbol{\beta} + \Lambda\boldsymbol{\eta}_i) + \boldsymbol{\epsilon}_i,$$

$$\boldsymbol{\eta}_i \sim N_L(\mathbf{0}_L, I_L), \quad \boldsymbol{\epsilon}_i \sim N_T(\mathbf{0}_T, \sigma^2_\epsilon I_T), \quad i = 1, \ldots, n,$$
$$\boldsymbol{\beta} \sim N_R\left(\mathbf{0}_R, \frac{1}{\sigma^2_\beta}\Omega^{-1}\right), \quad \sigma^2_\beta \sim \text{Gamma}\left(\frac{a_\beta}{2}, \frac{a_\beta}{2}\right), \quad \frac{1}{\sigma^2_\epsilon} \propto c$$
$$\boldsymbol{\lambda}_\ell \sim N_R\left(\mathbf{0}_R, \Sigma_{\lambda_\ell}\right), \quad \Sigma_{\lambda_\ell} = \text{diag}(\sigma^2_{\lambda_{1\ell}}, \ldots, \sigma^2_{\lambda_{R\ell}}), \quad \sigma^2_{\lambda_{r\ell}} = \varphi^{-1}_{r\ell}\tau^{-1}_\ell,$$
$$\varphi_{r\ell} \sim \text{Gamma}\left(\frac{\nu}{2}, \frac{\nu}{2}\right), \quad \tau_\ell = \prod_{h=1}^{\ell}\delta_h, \quad \delta_1 \sim \text{Gamma}(a_1, 1),\ \delta_h \sim \text{Gamma}(a_2, 1)I(\delta_h > 1),\ h \geq 2.$$

Let $\widetilde{\boldsymbol{\Lambda}} = \text{Vec}(\Lambda)$ be the $RL \times 1$ vector stacking the L columns of Λ and $H_\epsilon = 1/\sigma^2_\epsilon$. The full conditional distributions are as follows:

1. $\boldsymbol{\beta}|\text{others} \sim N_R(\boldsymbol{\mu}^{post}_\beta, v^{post}_\beta)$ where $v^{post}_\beta = (1/n)\{B^\top\Sigma^{-1}_y B + (\sigma^2_\beta/n)\Omega\}^{-1}$, $\boldsymbol{\mu}^{post}_\beta = v^{post}_\beta \times nB^\top\Sigma^{-1}_y\overline{\boldsymbol{Y}}$, where $\Sigma^{-1}_y = B\Lambda\Lambda^\top B^\top + \sigma^2_\epsilon I_T$ and $\overline{\boldsymbol{Y}} = \frac{1}{n}\sum_{i=1}^n \boldsymbol{Y}_i$.

2. $\widetilde{\boldsymbol{\Lambda}}|\text{others} \sim N_{RL}(\boldsymbol{\mu}^{post}_\Lambda, v^{post}_\Lambda)$ where $v^{post}_\Lambda = \sigma^2_\epsilon\{(\sum_{i=1}^n \boldsymbol{\eta}_i\boldsymbol{\eta}_i^\top) \otimes B^\top B + \sigma^2_\epsilon\Sigma^{-1}_\Lambda\}^{-1}$, $\boldsymbol{\mu}^{post}_\Lambda = v^{post}_\Lambda \times (1/\sigma^2_\epsilon)\sum_{i=1}^n(\boldsymbol{\eta}_i^\top \otimes B)^\top\boldsymbol{Y}^c_i$, where $\otimes$ is the Kronecker product, Σ_Λ is a diagonal

matrix, denoted as $\Sigma_\Lambda = \text{diag}(\varphi_{11}^{-1}\tau_1^{-1}, \ldots, \varphi_{R1}^{-1}\tau_1^{-1}, \ldots, \varphi_{1L}^{-1}\tau_L^{-1}, \ldots, \varphi_{RL}^{-1}\tau_L^{-1})$, and $\boldsymbol{Y}_i^c = \boldsymbol{Y}_i - B\boldsymbol{\beta}$.

3. $H_\epsilon|\text{others} \sim \text{Gamma}(a_{\sigma_\epsilon^2}^{post}, b_{\sigma_\epsilon^2}^{post})$, where $a_{\sigma_\epsilon^2}^{post} = (nT)/2$, $b_{\sigma_\epsilon^2}^{post} = RSS/2$, and $RSS = \sum_{i=1}^n \{\boldsymbol{Y}_i - B(\boldsymbol{\beta} + \Lambda\boldsymbol{\eta}_i)\}^\top \{\boldsymbol{Y}_i - B(\boldsymbol{\beta} + \Lambda\boldsymbol{\eta}_i)\}$.

4. $\boldsymbol{\eta}_i|\text{others} \sim N_L(\boldsymbol{\mu}_{\eta_i}^{post}, v_{\eta_i}^{post})$, where $v_{\eta_i}^{post} = \sigma_\epsilon^2(\Lambda^\top B^\top B\Lambda + \sigma_\epsilon^2 I_L)^{-1}$, $\boldsymbol{\mu}_{\eta_i}^{post} = v_{\eta_i}^{post} \times (1/\sigma_\epsilon^2)\Lambda^\top B^\top(\boldsymbol{Y}_i - B\boldsymbol{\beta})$, for $i = 1, \ldots, n$.

5. $\sigma_\beta^2|\text{others} \sim \text{Gamma}(a_{\sigma_\beta^2}^{post}, b_{\sigma_\beta^2}^{post})$, where $a_{\sigma_\beta^2}^{post} = (R + a_\beta)/2$, $b_{\sigma_\beta^2}^{post} = (a_\beta + \boldsymbol{\beta}^\top\Omega\boldsymbol{\beta})/2$

6. $\varphi_{r\ell}|\text{others} \sim \text{Gamma}(a_{\varphi_{r\ell}}^{post}, b_{\varphi_{r\ell}}^{post})$, where $a_{\varphi_{r\ell}}^{post} = (\nu + 1)/2$, $b_{\varphi_{r\ell}}^{post} = (\nu + \tau_\ell\lambda_{r\ell}^2)/2$.

7. $\tau_\ell|\text{others} = \prod_{h=1}^\ell \delta_h|\text{others}$

   (a) $\delta_1|\text{others} \sim \text{Gamma}(a_{\delta_1}^{post}, b_{\delta_1}^{post})$, where $a_{\delta_1}^{post} = a_1 + (1/2)RL$, $b_{\delta_1}^{post} = 1 + (\gamma_1 + \sum_{\ell=2}^L \zeta_\ell^{(1)}\gamma_\ell)/2$, where $\zeta_\ell^{(1)} = \prod_{h=2}^\ell \delta_h$ and $\gamma_\ell = \sum_{r=1}^R \varphi_{r\ell}\lambda_{r\ell}^2$.

   (b) $\delta_h|\text{others} \sim \text{Gamma}(a_{\delta_h}^{post}, b_{\delta_h}^{post})I(\delta_h \geq 1)$, $h \geq 2$, where $a_{\delta_h}^{post} = a_2 + R(L - h + 1)/2$, $b_{\delta_h}^{post} = 1 + (\gamma_h + \sum_{\ell=(h+1)}^L \zeta_\ell^{(h)}\gamma_\ell)/2$, and $\zeta_\ell^{(h)} = \prod_{h' \neq h} \delta_{h'}$.

A Gibbs sampler is used to sample from the posterior distributions given above. For the variance component σ_β^2, the hyperparameter for the prior is set to $a_\beta = 2$. For the factor loading matrix, the hyperparameter of the prior for $\varphi_{r\ell}$ is set to $\nu = 10$, and the hyperparameters of the priors for τ_ℓ are set to $a_1 = 1$ and $a_2 = 2$. A small constant $\varsigma = 0.00001$ is added to the diagonal elements of the penalty matrix Ω to guarantee positive-definiteness, where Ω is an $R \times R$ matrix with elements

$$\Omega = \begin{bmatrix} 1 & -1 & 0 & \ldots & \ldots & 0 \\ -1 & 2 & -1 & 0 & \ldots & 0 \\ 0 & -1 & 2 & -1 & \ldots & 0 \\ \vdots & \ddots & \ddots & \ddots & \ddots & \vdots \\ 0 & \ldots & 0 & -1 & 2 & -1 \\ 0 & \ldots & \ldots & 0 & -1 & 1 \end{bmatrix} + \varsigma I_R,$$

and I_R denotes the $R \times R$ identity matrix.

Appendix B. Alignment of Eigenfunction Estimates

Let $\psi_k^{(m)}(t)$ denote the mth posterior sample, $m = 1, \ldots, M$, of the kth eigenfunction, $\psi_k(t)$, $k = 1, \ldots, K$. To align the sign of the eigenfunction estimates across the MCMC samples, we utilize the below alignment algorithm. In the proposed alignment algorithm, $\{\psi_k^{(1)^\star}(t), \ldots, \psi_k^{(M)^\star}(t)\}$ denotes the aligned posterior sample with $\psi_k^{(m)^\star}(t) = a^{(m)}\psi_k^{(m)}(t)$ and $a^{(m)} \in \{-1, 1\}$, and $\overline{\psi}_k^{(m)}(t) = (1/m)\sum_{j=1}^{m} \psi_k^{(j)^\star}(t)$ denotes the ergodic mean of the aligned sample.

Algorithm 1 Alignment of the posterior eigenfunctions

Step 1: Set $a^{(1)} = 1$ and $\psi_k^{(1)^\star} = \psi_k^{(1)}$.
Step 2: For $m = 2, \ldots, M$;

a. Calculate the aligned ergodic mean $\overline{\psi}_k^{(m-1)}(t)$ and compute

$$d_+^{(m)} := \int \left| \overline{\psi}_k^{(m-1)}(t) - \psi_k^{(m)}(t) \right| dt,$$

and

$$d_-^{(m)} := \int \left| \overline{\psi}_k^{(m-1)}(t) + \psi_k^{(m)}(t) \right| dt.$$

b. Set

$$a^{(m)} = I\left(d_+^{(m)} \leq d_-^{(m)}\right) - I\left(d_+^{(m)} > d_-^{(m)}\right),$$

and $\psi_k^{(m)^\star}(t) = a^{(m)}\psi_k^{(m)}(t)$, where $I(\cdot)$ denotes the indicator function.

Appendix C. Simulation Cases and Additional Simulation Results

Five simulation scenarios are considered to display the use of CPEs in describing the variation in the posterior samples in the presence of additional variation incorporated to the i.i.d functional sample (results given in main paper Section 4).

Case 1 (no additional variation): For case 1 with no added variation, a sample of functional data are generated according to the FPCA model with $K = 2$ eigencomponents. More specifically, functional data is generated according to $Y_i(t_j) = \mu(t_j) + \sum_{k=1}^{K} \xi_{ik}\psi_k(t_j) + \epsilon_i(t_j)$, for

$i = 1, \ldots, n = 50$ subjects at an equidistant grid of $j = 1, \ldots, T = 40$ time points in the unit interval 0 to 1. The mean function and the two mutually orthonormal eigenfunctions equal $\mu(t) = 10\sqrt{1 - 2(t - 0.5)^2}$, $\psi_1(t) = \sqrt{2}\sin(2\pi t)$ and $\psi_2(t) = \sqrt{2}\cos(2\pi t)$, respectively. The subject-specific FPCA scores, $(\xi_{i1}, \xi_{i2})^\top$, are generated from independent normal distributions with mean zero and variances $\rho_1 = 15$ and $\rho_2 = 5$, respectively. Lastly, the measurement error, $\epsilon_i(t_j)$, is generated independently from $N(0, \sigma_\epsilon^2)$ with $\sigma_\epsilon^2 = 15$.

Case 2 (additional constant variation): Case 2 generates observations with added variation by adding a constant deviation to the mean function (with a random sign): $Z_i(t) = Y_i(t) + \omega_i W(t)$ for $t > T_i$ and $Z_i(t) = Y_i(t)$ for $t < T_i$, where $T_i \sim \text{Unif}[0, 1]$, $W(t) = 20, t \in [0, 1]$, and ω_i is generated as a discrete variable with values -1 or 1 with probability $1/2$.

Case 3 (variation added through eigenvalues): Case 3 generates observations with additional variation using larger eigenvalues: $Z_i(t) = \mu(t) + \sum_{k=1}^{2} \zeta_{ik}\psi_k(t) + \epsilon_i(t)$, where ζ_{i1} and ζ_{i2} are generated independently from $N(0, 30)$ and $N(0, 20)$, respectively.

Case 4 (variation added through time-shifted eigenfunctions): Case 4 generates observations with additional variation using: $Z_i(t) = \mu(t) + \sum_{k=1}^{2} \xi_{ik}\kappa_k(t) + \epsilon_i(t)$, where $\kappa_1(t) = \sqrt{2}\sin\{2\pi(t - 0.25)\}$ and $\kappa_2(t) = \sqrt{2}\cos\{2\pi(t - 0.25)\}$.

Case 5 (variation added through higher-frequency eigenfunctions): For case 5, observations with additional variation are generated according to $Z_i(t) = \mu(t) + \sum_{k=1}^{2} \xi_{ik}\kappa_k(t) + \epsilon_i(t)$, where $\kappa_1(t) = \sqrt{2}\sin\{4\pi t\}$ and $\kappa_2(t) = \sqrt{2}\cos\{4\pi t\}$.

In Cases 2 through 5, the percentage of observations with additional variation (denoted by $Z_i(t)$) equals $q = 10$ or 20% of the functional sample. For each simulation case with added variation, the 'true' eigenfunctions and eigenvalues (for IMSE and MSE calculations) are derived from the overall covariance, calculated as the weighted sum of the covariance of the original sample (denoted by $Y_i(t)$) and the covariance of the observations with additional variation (denoted by $Z_i(t)$). The computational time for creating MBD and MVD-CPEs with

a total of 10 α-level cutoffs are 0.08 and 1.10 seconds, respectively.

Finite sample performance of point estimates of the functional model components (i.e. mean and eigenfunctions) and scalar model components (i.e. eigenvalues) are assessed via the standardized integrated mean squared error (IMSE), $IMSE_{\widehat{g}(t)} = [\int_t \{\widehat{g}(t) - g(t)\}^2 dt] / \int_t g^2(t) dt$, and the standardized mean squared error (MSE), $MSE_{\widehat{\rho_k}} = (\widehat{\rho}_k - \rho_k)^2 / \rho_k^2$, respectively. The mean IMSE and MSE values from 200 Monte Carlo runs for the five simulation scenarios are summarized in Supplementary Materials Table S2. The traditional and proposed point estimates for the mean function and the three leading eigenfunctions from the Monte Carlo run with the median IMSE are given in Supplementary Materials Figure S2, S3, S4 and S5, respectively. In addition, Supplementary Materials Figure S6, Figures 1, 2 and Figure S7 display CPEs from α cutoffs ranging from 0.05 to 0.95 for the mean function and the leading three eigenfunctions, respectively, from a single Monte Carlo run overlaying $M = 4,000$ posterior estimates (given in gray) for the five simulation scenarios (for $q = 20\%$).

The first simulation scenario of with no additional variation shows that the traditional point estimates ($\widehat{\psi}_k(t)$ and $\widetilde{\psi}_k(t)$) perform quite well (yielding small IMSE and MSE values) compared to their depth based counter parts ($\widehat{m}\{\psi_k(t)\}$ and $\widetilde{m}\{\psi_k(t)\}$) (Supplementary Materials Table S2). The traditional summaries obtained by averaging posterior samples, while having a larger bias than depth-based measures, have smaller variances compared to depth-based measures, leading to smaller IMSE and MSE values consistently across the different simulation cases. The observations with additional variation in the second simulation scenario add a constant deviation from the mean function over a random portion of the time domain ($t \in [T_i, 1]$) with a random sign. Due to the random sign of the constant deviation, rather than biasing the mean function, they increase the variation in the mean function estimation (IMSE values for mean estimation are higher for Case 2 than other simulation scenarios in Supplementary Materials Table S2). Case 3 generates observations with larger eigenvalues, which increase the variation

along the eigenfunctions. Due to the shapes of the eigenfunctions considered this adds variation across the entire unit interval, as is detected through the CPEs in Figures 1 and 2. While this additional variation does not bias the point estimates (except for ρ_k), the IMSE in estimation of the eigenfunctions are slightly higher than Case 1 with no additional variation. Finally, Cases 4 and 5 consider additional variation through eigenfunctions where added observations are generated under altered eigenfunctions: in Case 4 eigenfunctions are shifted in time, in Case 5 the frequency of the eigenfunctions is increased. Both cases lead to additional variation in estimation of the eigenfunctions (consistent with higher IMSE values for targeting $\psi_k(t)$ compared to Case 1 in Supplementary Materials Table S1). More specifically, while the time shift in the eigenfunctions adds variation to eigenfunction estimation throughout the unit interval in Case 4, the added variation due to higher frequency eigenfunctions is apparent especially in Figures 2 (i) and (j) with higher frequency posterior estimates of $\psi_2(t)$ captured in the $\alpha = 0.95$ MBD-CPEs and $\alpha = 0.25$ MVD-CPEs.

Appendix D. EEG Data

Our motivating study collected electroencephalogram (EEG) data sampled at 500Hz for 2 minutes using a 128-channel HydroCel Geodesic Sensor Net on 58 children with autism spectrum disorder (ASD) and 39 of their typically developed (TD) peers. Four electrodes near the eyes were removed prior to recording to improve the comfort of the participants. The data was then interpolated to the international 10-20 system 25 channel montage via spherical interpolation, and independent component analysis (ICA) was used for identification of artifacts. Specifically, the EEG signals were reconstructed without components attributed to nonneural sources of the signals, such as the electromyogram (EMG) or other non-stereotyped artifacts, and then re-referenced to an average of all channels. The first 38 seconds of the artifact-free EEG data was used for each subject for spectral power analysis as the 38 seconds of the recordings rep-

resented the minimum amount of artifact-free data available across all participants and was deemed an appropriate minimum threshold to gain reliable estimates of the signals following previous literature. Spectral density estimates of the 38 second EEG recordings were obtained using Welch's method by dividing the data into 2-second Hanning windows with 50% overlap and transforming into the frequency domain via a fast Fourier transformation (FFT). For each electrode, the spectral densities were averaged at each overlapping segment, resulting in electrode-specific estimates of the spectral density, which were then averaged across the 25 electrodes to obtain scalp-wide spectral densities for each participant.

Table S1: Notation used for point estimates for the BFPCA components (mean function $\mu(t)$, eigenfunction $\psi_k(t)$, eigenvalue ρ_k and covariance $C(s,t)$) and credible intervals for $\mu(t)$ and $\psi_k(t)$ obtained from traditional summaries as well as the proposed CPEs.

	Traditional Summaries			Proposed Summaries			
BFPCA Components	Point Estimates	Credible Intervals		Point Estimates	Central Posterior Envelopes (CPEs)		
$\mu(t)$	$\widehat{\mu}(t)$	$P_1^p - \alpha\{\mu(t)\}$ $P_1^s - \alpha\{\mu(t)\}$ $Q_1^p - \alpha\{\mu(t)\}$ $Q_1^s - \alpha\{\mu(t)\}$	Pointwise parametric Simultaneous parametric Pointwise quantile Simultaneous quantile	$\widehat{m}\{\mu(t)\}$	MBD median	$D_{1-\alpha}\{\mu(t)\}$	MBD-CPE
$\psi_k(t)$	$\widehat{\psi}_k(t)$	$P_1^p - \alpha\{\psi_k(t)\}$ $P_1^s - \alpha\{\psi_k(t)\}$ $Q_1^p - \alpha\{\psi_k(t)\}$ $Q_1^s - \alpha\{\psi_k(t)\}$	Pointwise parametric Simultaneous parametric Pointwise quantile Simultaneous quantile	$\widehat{m}\{\psi_k(t)\}$	MBD median	$D_{1-\alpha}\{\psi_k(t)\}$	MBD-CPE
	$\widetilde{\psi}_k(t)$			$\widetilde{m}\{\psi_k(t)\}$	MVD median	$D^{\star}_{1-\alpha}\{\psi_k(t)\}$	MVD-CPE
ρ_k	$\widehat{\rho}_k$ $\widetilde{\rho}_k$						
$C(s,t)$	$\widetilde{C}(s,t)$						

Table S2: The mean standardized integrated mean squared error (IMSE) and standardized mean squared error (MSE) for both the traditional and functional depth-based point estimates from the 200 Monte Carlo runs. The five simulation cases correspond to: Case 1 – no additional variation, Case 2 – additional constant variation, Case 3 – variation added through eigenvalues, Case 4 – variation added through time-shifted eigenfunctions, Case 5 – variation added through higher-frequency eigenfunctions with $q = \{10, 20\}\%$ of observations with additional variation.

		$q = 10\%$				$q = 20\%$			
Point Estimate	Case 1	Case 2	Case 3	Case 4	Case 5	Case 2	Case 3	Case 4	Case 5
	IMSE	**IMSE**				**IMSE**			
$\widehat{\mu}(t)$	0.0034	0.0084	0.0046	0.0037	0.0042	0.0110	0.0051	0.0035	0.0038
$\widehat{m}\{\mu(t)\}$	0.0037	0.0088	0.0048	0.0040	0.0044	0.0116	0.0054	0.0038	0.0041
$\widehat{\psi}_1(t)$	0.0230	0.1568	0.0485	0.0463	0.0299	0.0663	0.0625	0.0813	0.0395
$\widetilde{\psi}_1(t)$	0.0226	0.1667	0.0468	0.0467	0.0300	0.0663	0.0646	0.0805	0.0392
$\widehat{m}\{\psi_1(t)\}$	0.0262	0.1802	0.0516	0.0506	0.0347	0.0710	0.0680	0.0873	0.0445
$\widetilde{m}\{\psi_1(t)\}$	0.0276	0.1812	0.0545	0.0556	0.0372	0.0762	0.0692	0.0876	0.0502
$\widehat{\psi}_2(t)$	0.0392	0.3948	0.0605	0.0583	0.0751	0.1440	0.0722	0.0904	0.4209
$\widetilde{\psi}_2(t)$	0.0390	0.4240	0.0593	0.0592	0.0753	0.1504	0.0746	0.0904	0.4721
$\widehat{m}\{\psi_2(t)\}$	0.0470	0.4560	0.0671	0.0683	0.0913	0.1653	0.0821	0.0972	0.5021
$\widetilde{m}\{\psi_2(t)\}$	0.0566	0.4586	0.0773	0.0771	0.1072	0.1755	0.0872	0.1057	0.5339
$\widehat{\psi}_3(t)$	-	0.2865	-	-	0.3290	0.1345	-	-	0.5255
$\widetilde{\psi}_3(t)$	-	0.3172	-	-	0.3659	0.1432	-	-	0.5955
$\widehat{m}\{\psi_3(t)\}$	-	0.3300	-	-	0.4100	0.1521	-	-	0.6409
$\widetilde{m}\{\psi_3(t)\}$	-	0.3599	-	-	0.4652	0.1761	-	-	0.6851
	MSE	**MSE**				**MSE**			
$\widehat{\rho}_1$	0.1198	0.1043	0.1096	0.1025	0.1036	0.1782	0.1066	0.0861	0.0961
$\widetilde{\rho}_1$	0.1313	0.1235	0.1208	0.1158	0.1160	0.1931	0.1187	0.1024	0.1130
$\widehat{\rho}_2$	0.0828	0.1095	0.1219	0.1157	0.0711	0.0971	0.1345	0.1422	0.0362
$\widetilde{\rho}_2$	0.0836	0.1173	0.1202	0.1127	0.0820	0.1020	0.1299	0.1342	0.0544
$\widehat{\rho}_3$	-	0.1261	-	-	0.1417	0.0870	-	-	0.1039
$\widetilde{\rho}_3$	-	0.1104	-	-	0.1884	0.0776	-	-	0.1001

Table S3: Results from the regression of the first two leading FPCA scores onto diagnostic group (ASD), age (centered– in months) and the interaction between age and diagnostic group. For each variable, the estimated regression coefficient $\widehat{\beta}$, the corresponding standard error and p-value are given.

	FPCA scores $k = 1$		FPCA scores $k = 2$	
Variable	$\widehat{\beta}$ (SE)	p-value	$\widehat{\beta}$ (SE)	p-value
Intercept	0.0094 (0.0059)	0.1106	0.0016 (0.0036)	0.6555
Group (ASD)	-0.0162 (0.0076)	0.0354*	-0.0022 (0.0047)	0.6343
Age (months)	0.0006 (0.0002)	0.0124*	-0.0008 (0.0001)	<0.0001***
Group×Age	-0.0004 (0.0003)	0.1813	0.0006 (0.0002)	0.0016**

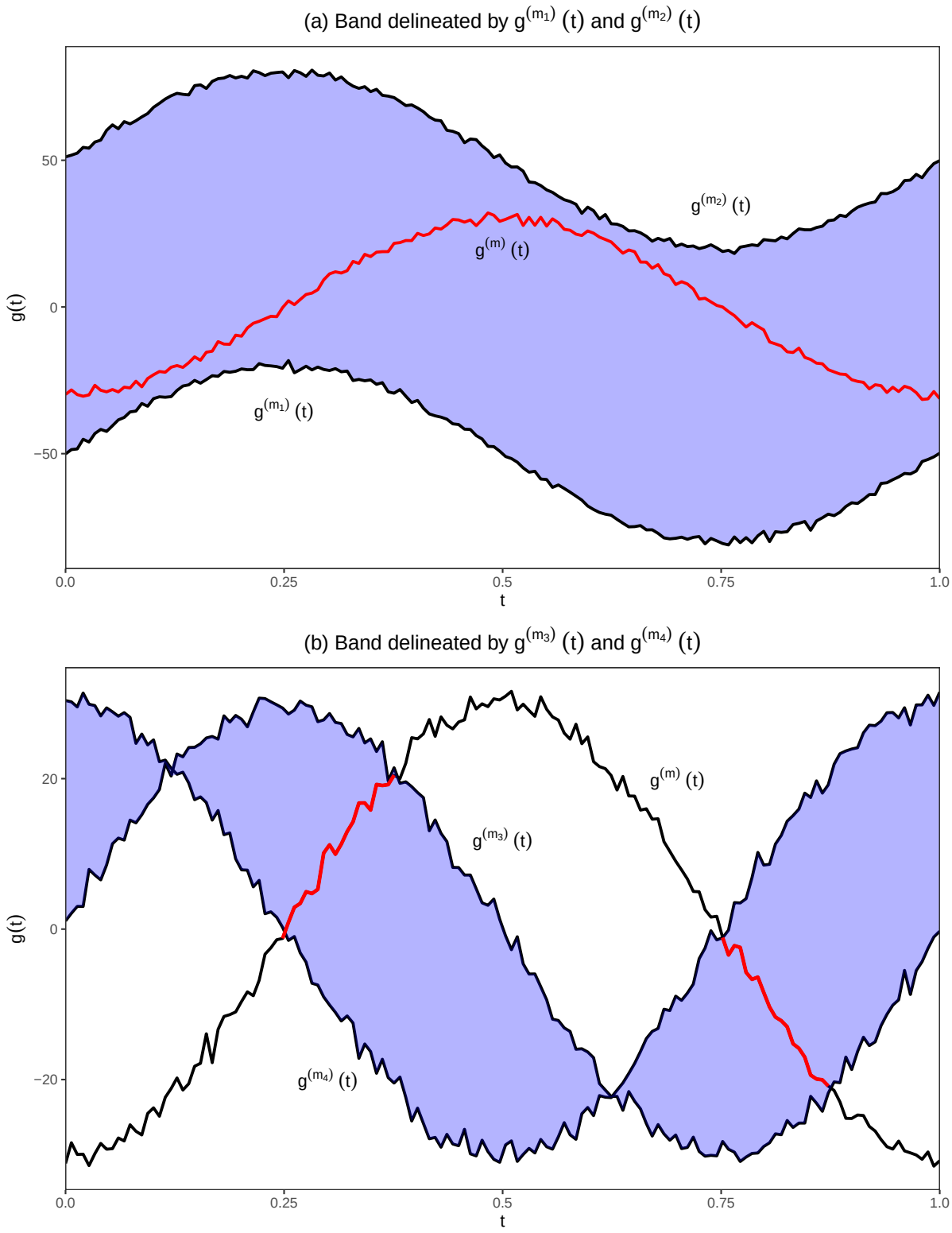

Figure S1: The bands given, $\mathcal{B}\left\{g^{(1)}(t), g^{(2)}(t)\right\}$ and $\mathcal{B}\left\{g^{(3)}(t), g^{(4)}(t)\right\}$, are represented as the blue shaded region. The proportion of the curve $g^{(m)}(t)$ that lies within the respective bands is given in red, where $\mathcal{A}_2^*\left\{g^{(m)}(t); g^{(1)}(t), g^{(2)}(t)\right\} = 1$ and $\mathcal{A}_2^*\left\{g^{(m)}(t); g^{(3)}(t), g^{(4)}(t)\right\} = 0.253$.

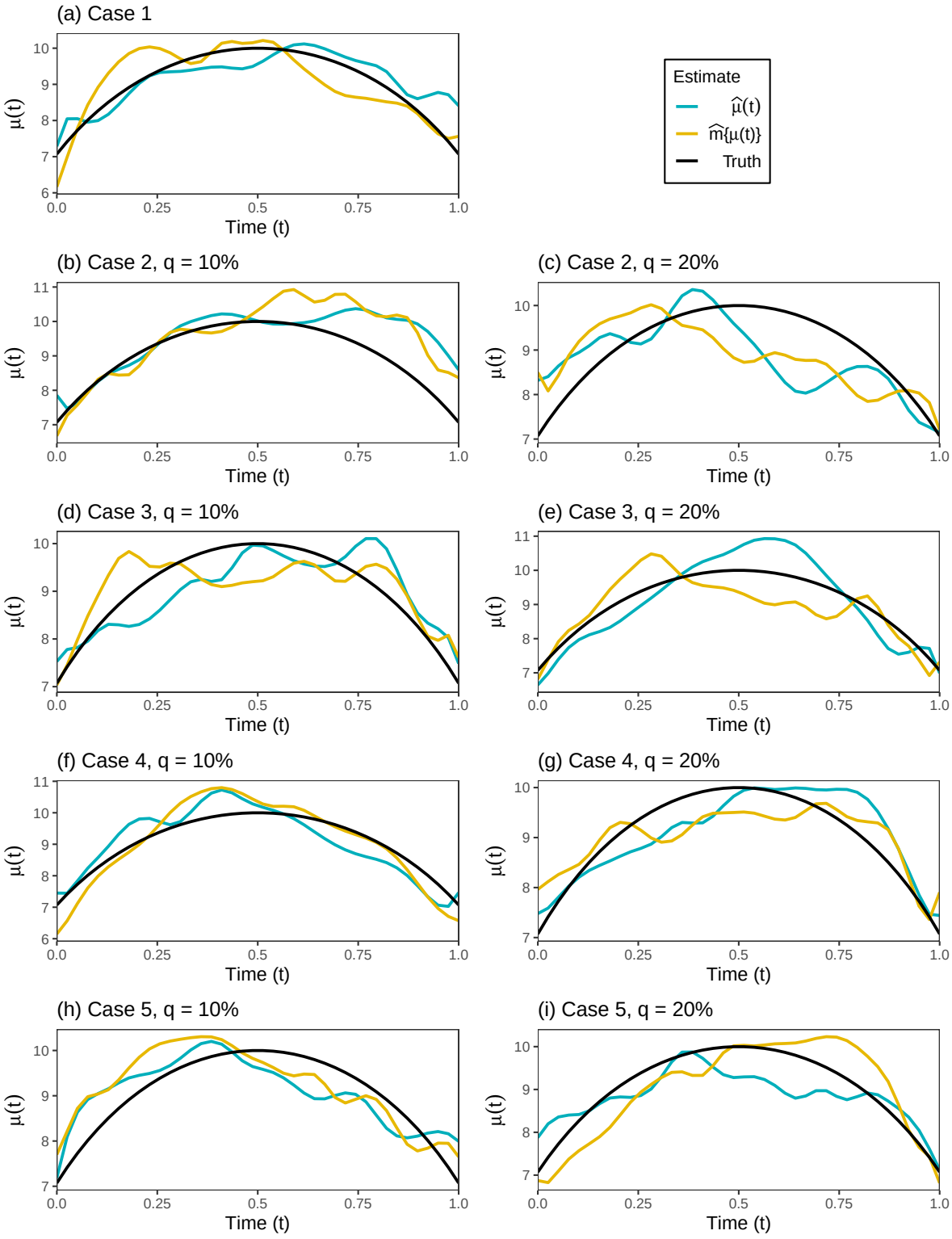

Figure S2: Point estimates of $\mu(t)$ for each simulation case with $q = 10$ and $q = 20\%$ of observations with added variation from runs with 50th percentile IMSE values. Mean estimate and MBD median are given in blue and solid yellow, respectively, overlaying the true function given in black.

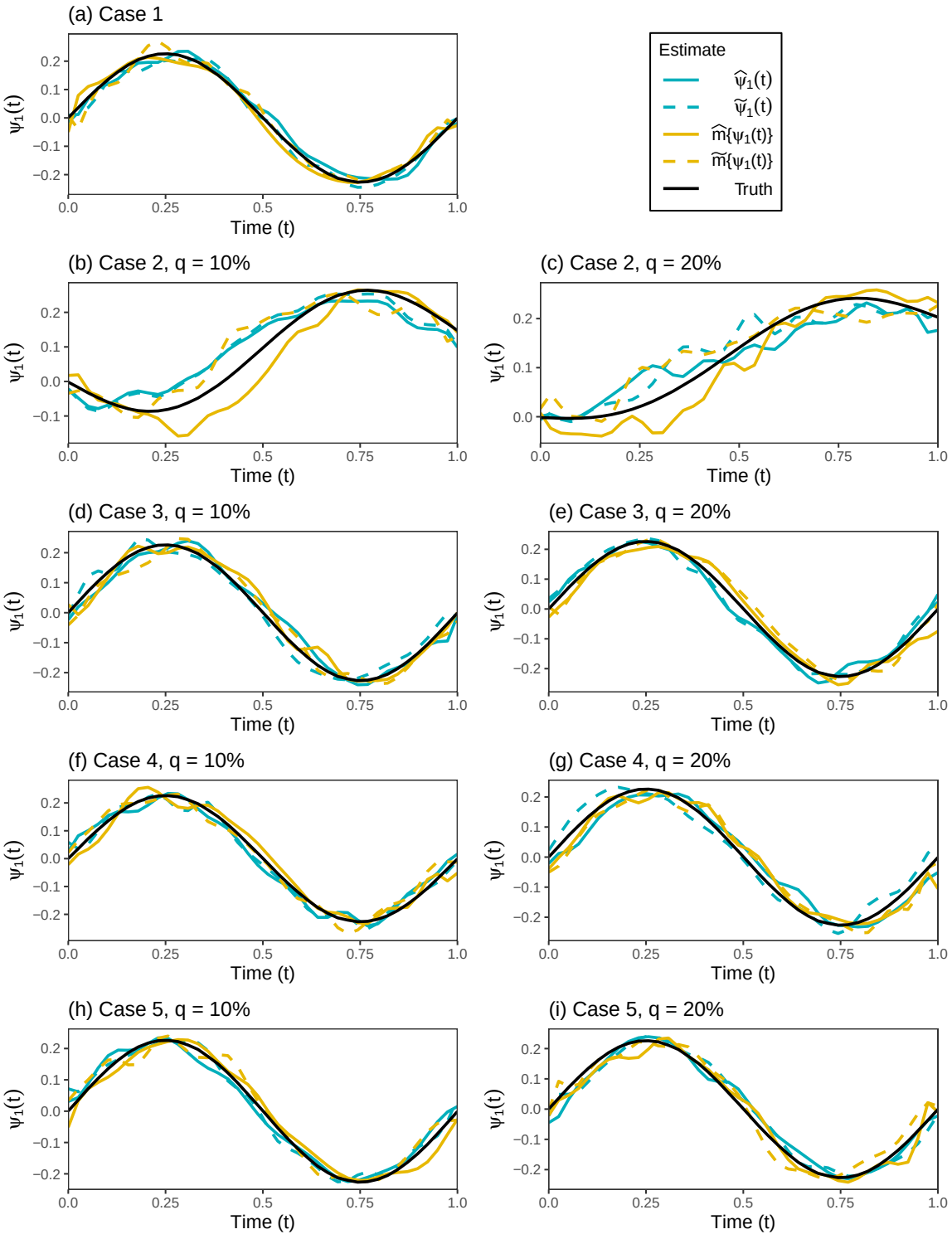

Figure S3: Point estimates of $\psi_1(t)$ for each simulation case with $q = 10$ and $q = 20\%$ of observations with added variation from runs with 50th percentile IMSE values. Eigenfunction estimates, eigenfunctions estimates via covariance estimation, MBD median and MVD median are given in solid blue, dashed blue, solid yellow and dashed yellow, respectively, overlaying the true function given in solid black.

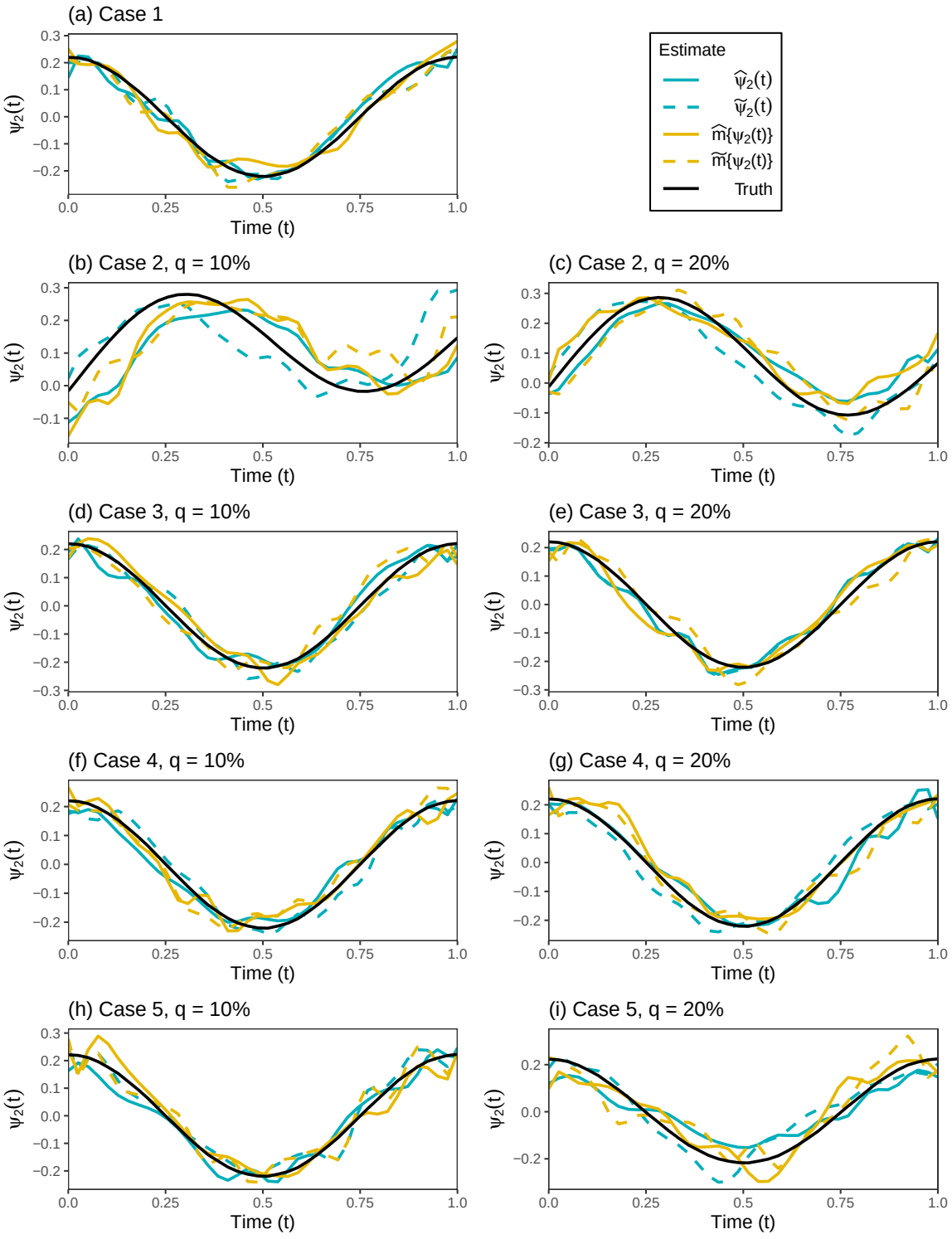

Figure S4: Point estimates of $\psi_2(t)$ for each simulation case with $q = 10$ and $q = 20\%$ of observations with added variation from runs with 50th percentile IMSE values. Eigenfunction estimates, eigenfunctions estimates via covariance estimation, MBD median and MVD median are given in solid blue, dashed blue, solid yellow and dashed yellow, respectively, overlaying the true function given in solid black.

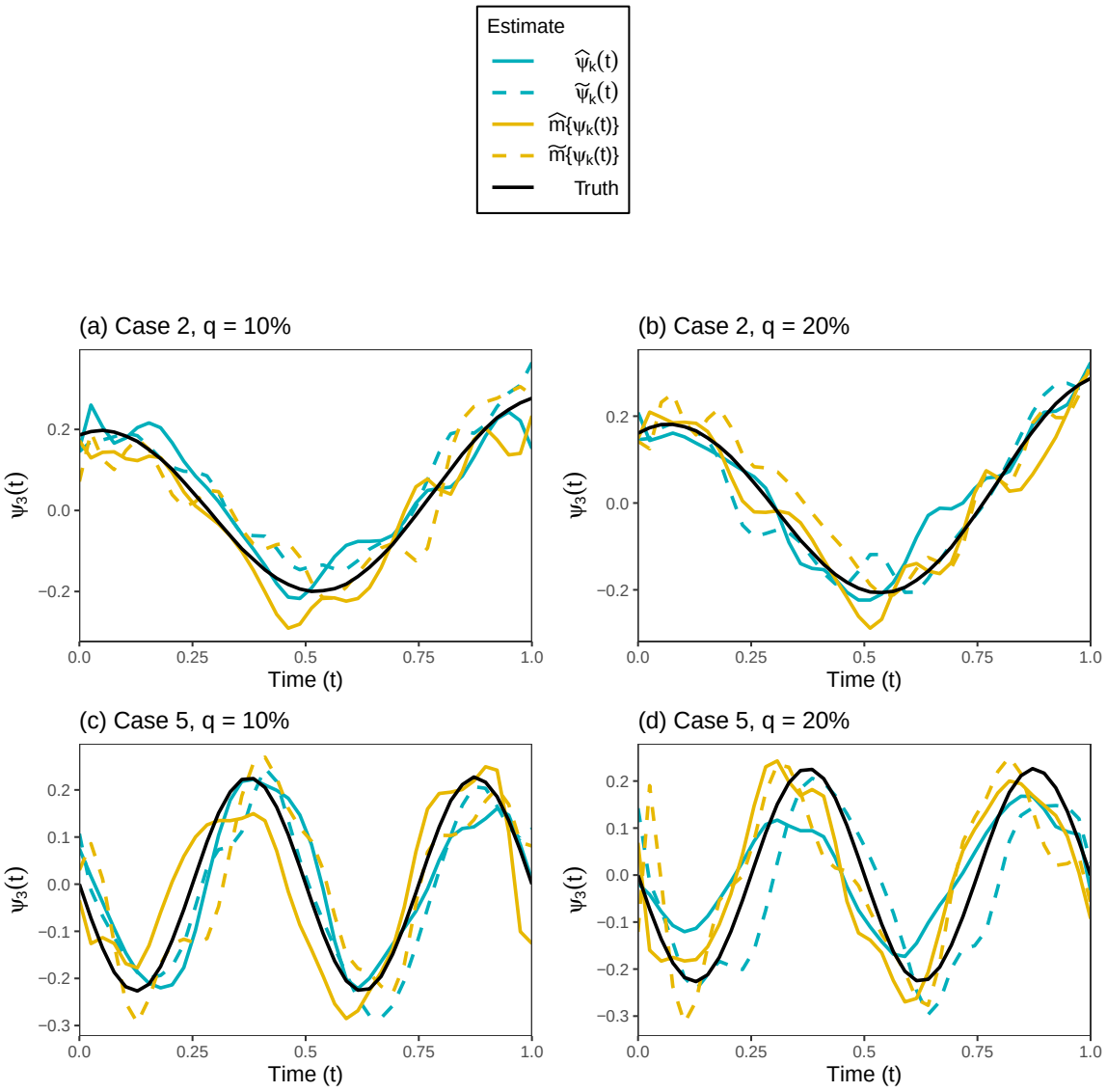

Figure S5: Point estimates of $\psi_3(t)$ for simulation Cases 2 and 5 with $q = 10$ and $q = 20\%$ of observations with added variation from runs with 50th percentile IMSE values. Eigenfunction estimates, eigenfunctions estimates via covariance estimation, MBD median and MVD median are given in solid blue, dashed blue, solid yellow and dashed yellow, respectively, overlaying the true function given in solid black.

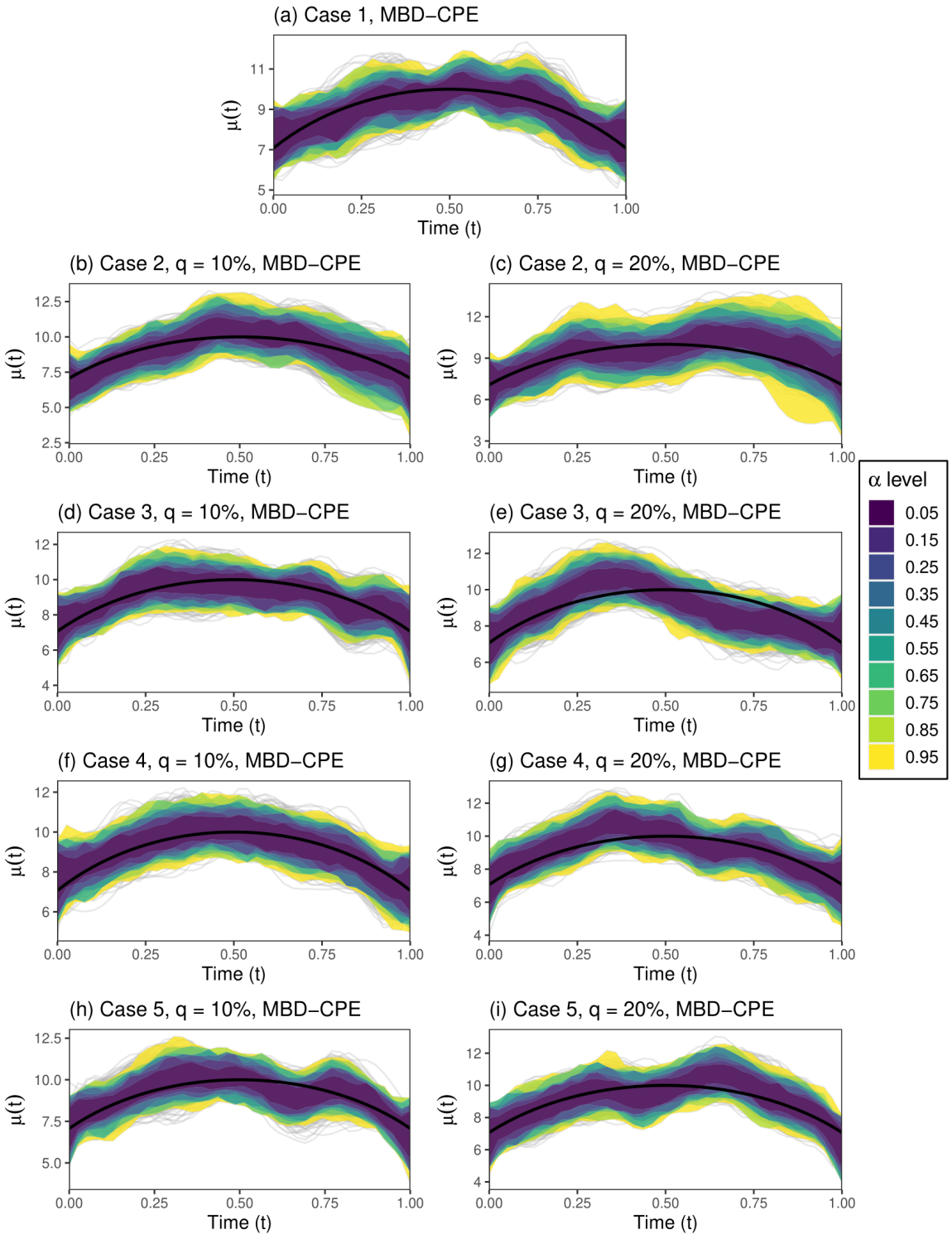

Figure S6: MBD-CPE contours of $\mu(t)$, denoted by $D_{1-\alpha}\{\mu(t)\}$, for each simulation case, overlaying the posterior estimates and the true function given in gray and black, respectively. The left and right hand columns (excluding the first row) display the MBD-CPEs for $q = 10\%$ and $q = 20\%$ of observations with added variation, respectively, at a grid of α levels marked by varying contour colors.

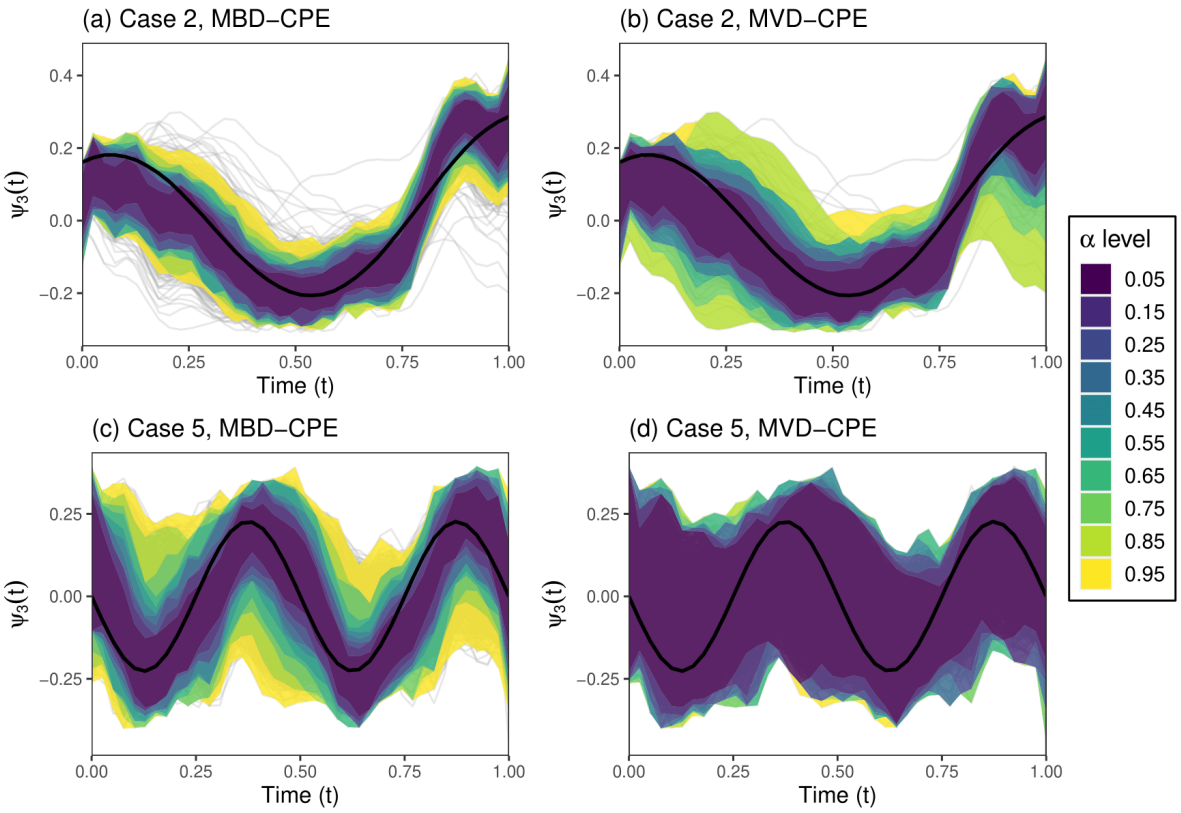

Figure S7: CPE contours of $\psi_3(t)$ for simulation Cases 2 and 5 with $q = 20\%$ of observations with added variation. The light grey solid lines, overlaying the true function in solid black, represent the sample of $M = 4000$ posterior estimates. The left and right hand columns display the MBD and MVD-CPEs, denoted by $D_{1-\alpha}\{\psi_1(t)\}$ and $D^{\star}_{1-\alpha}\{\psi_1(t)\}$, respectively, at a grid of α levels marked by varying contour colors.

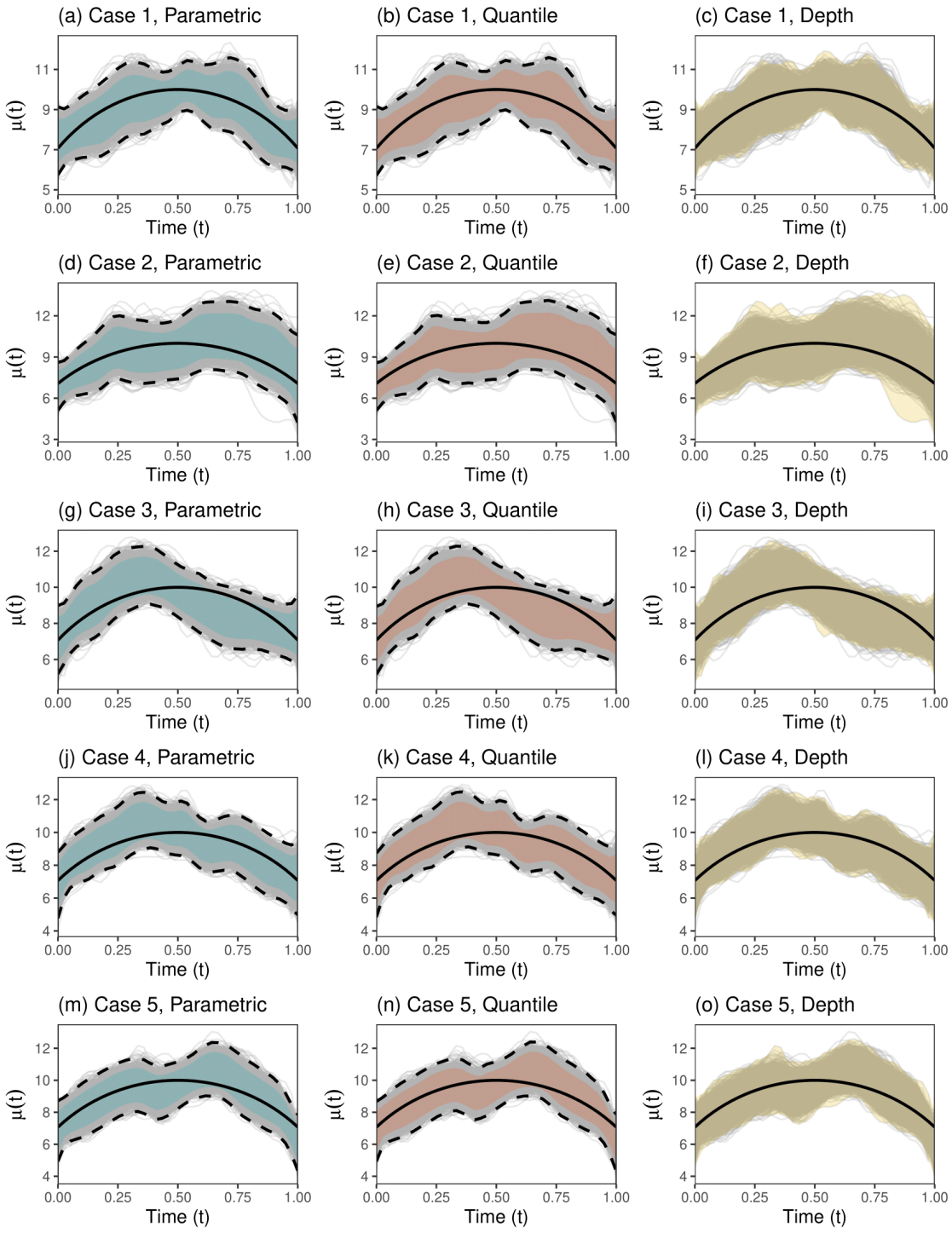

Figure S8: 95% parametric and quantile credible intervals along with 95% CPEs for $\mu(t)$ from a single Monte Carlo run for all simulation cases with $q = 20\%$ of observations with added variation. The light grey solid lines represent the sample of $M = 4000$ posterior estimates. The blue, red, and yellow shaded regions represent $P^p_{.95}\{\mu(t)\}$, $Q^p_{.95}\{\mu(t)\}$, and $D_{.95}\{\mu(t)\}$, respectively. The black dashed lines in the left and middle columns represent $P^s_{.95}\{\mu(t)\}$ and $Q^s_{.95}\{\mu(t)\}$, respectively, while the true function is given in solid black.

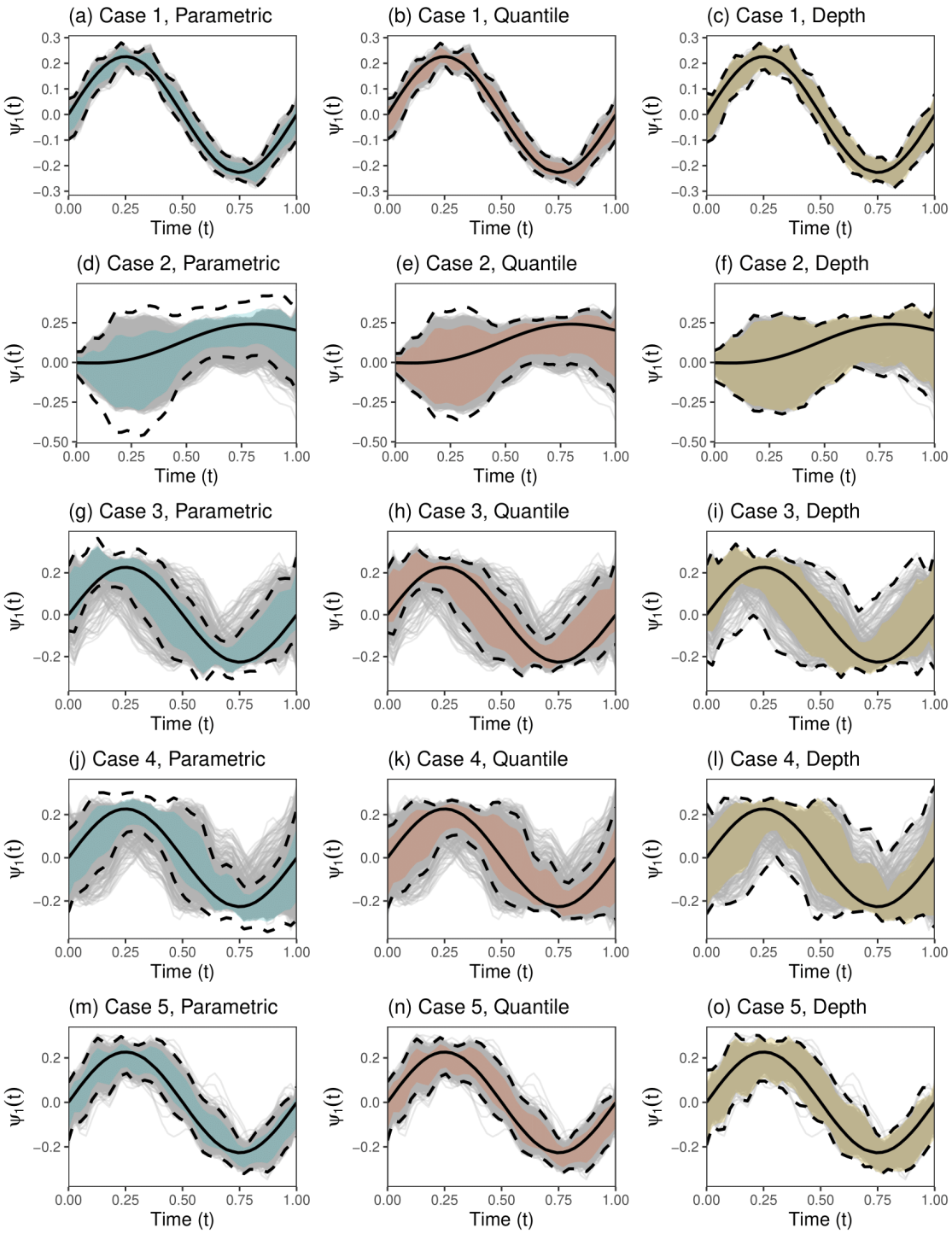

Figure S9: 95% parametric and quantile credible intervals along with 95% CPEs for $\psi_1(t)$ from a single Monte Carlo run for all simulation cases with $q = 20\%$ of observations with added variation. The light grey solid lines represent the sample of $M = 4000$ posterior estimates. The blue, red, and yellow shaded regions represent $P^p_{.95}\{\psi_1(t)\}$, $Q^p_{.95}\{\psi_1(t)\}$, and $D_{.95}\{\psi_1(t)\}$, respectively. The black dashed lines in the left, middle and right columns represent $P^s_{.95}\{\psi_1(t)\}$, $Q^s_{.95}\{\psi_1(t)\}$, and $D^\star_{.95}\{\psi_1(t)\}$, respectively, while the true function is given in solid black.

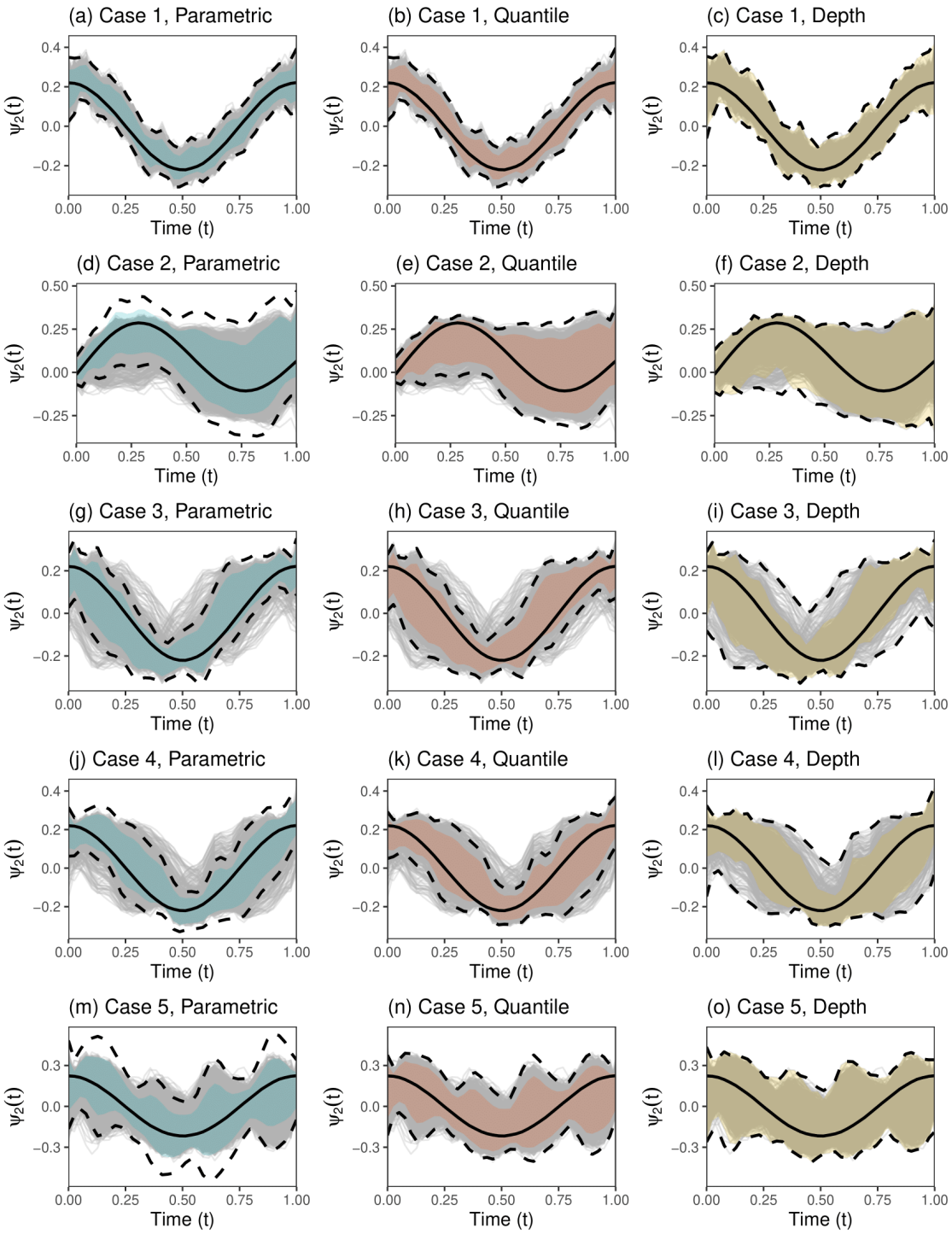

Figure S10: 95% parametric and quantile credible intervals along with 95% CPEs for $\psi_2(t)$ from a single Monte Carlo run for all simulation cases with $q = 20\%$ of observations with added variation. The light grey solid lines represent the sample of $M = 4000$ posterior estimates. The blue, red, and yellow shaded regions represent $P^p_{.95}\{\psi_2(t)\}$, $Q^p_{.95}\{\psi_2(t)\}$, and $D_{.95}\{\psi_2(t)\}$, respectively. The black dashed lines in the left, middle and right columns represent $P^s_{.95}\{\psi_2(t)\}$, $Q^s_{.95}\{\psi_2(t)\}$, and $D^\star_{.95}\{\psi_2(t)\}$, respectively, while the true function is given in solid black.

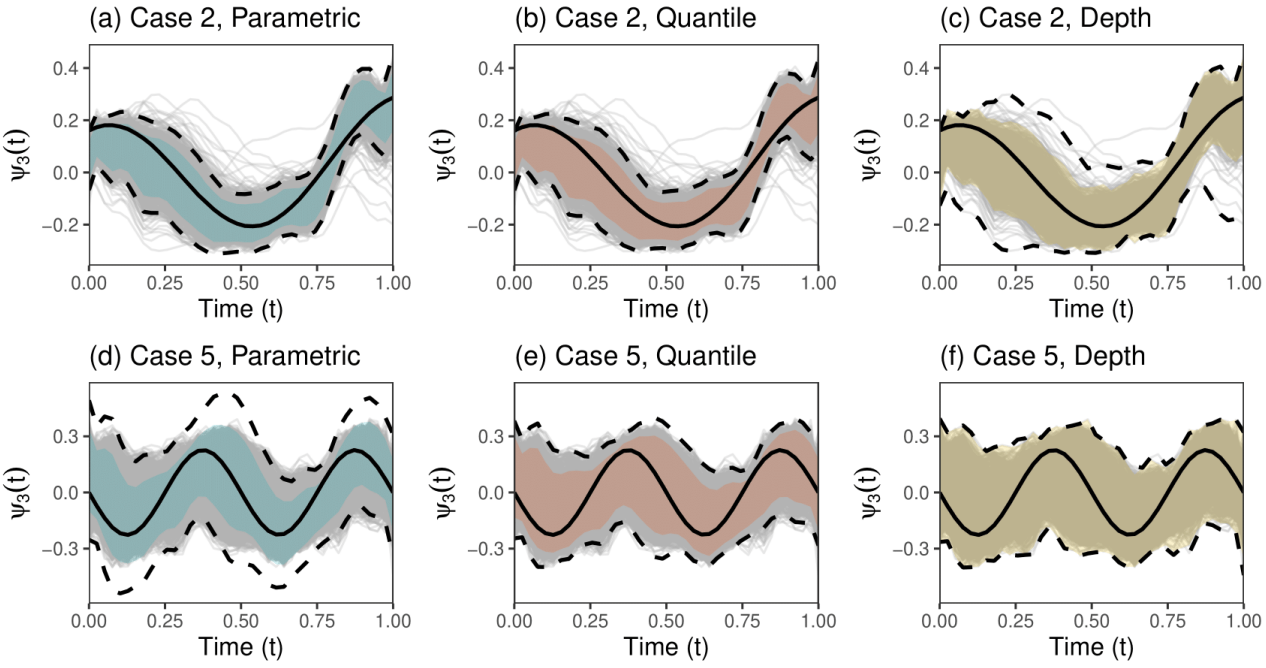

Figure S11: 95% parametric and quantile credible intervals along with 95% CPEs for $\psi_3(t)$ (Cases 2 and 5) from a single Monte Carlo run with $q = 20\%$ of observations with added variation. The light grey solid lines represent the sample of $M = 4000$ posterior estimates. The blue, red, and yellow shaded regions represent $P^p_{.95}\{\psi_2(t)\}$, $Q^p_{.95}\{\psi_2(t)\}$, and $D_{.95}\{\psi_2(t)\}$, respectively. The black dashed lines in the left, middle and right columns represent $P^s_{.95}\{\psi_2(t)\}$, $Q^s_{.95}\{\psi_2(t)\}$, and $D^\star_{.95}\{\psi_2(t)\}$, respectively, while the true function is given in solid black.

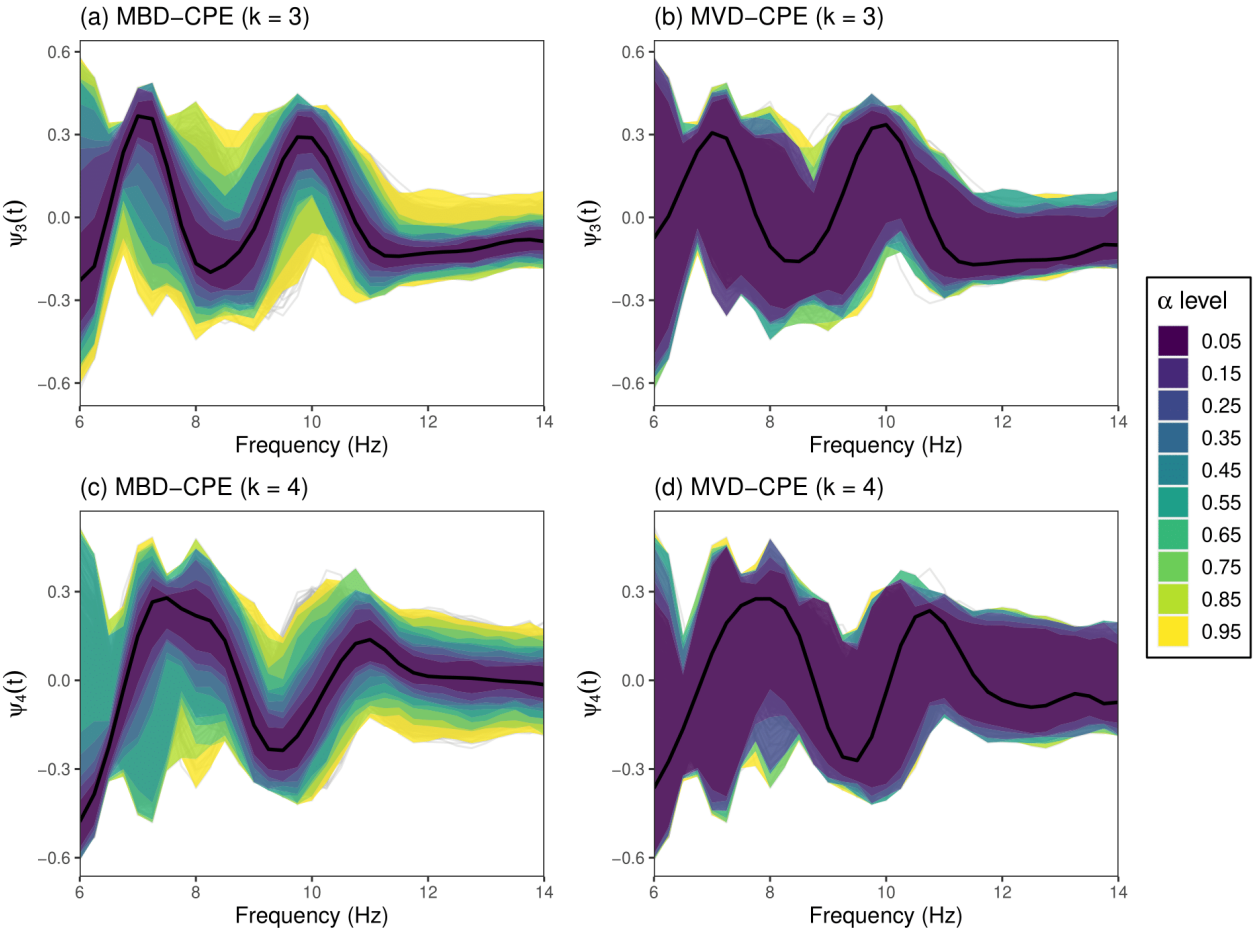

Figure S12: CPE contours of the third and fourth leading eigenfunctions for both ASD and TD groups in our data application, overlaying the posterior estimates given in gray. The left and right hand columns display the MBD and MVD-CPEs, denoted by $D_{1-\alpha}\{\psi_1(t)\}$ and $D^{\star}_{1-\alpha}\{\psi_1(t)\}$, respectively, at a grid of α levels marked by varying contour colors. The estimated MBD and MVD median are given in solid black in the right and left columns, respectively.

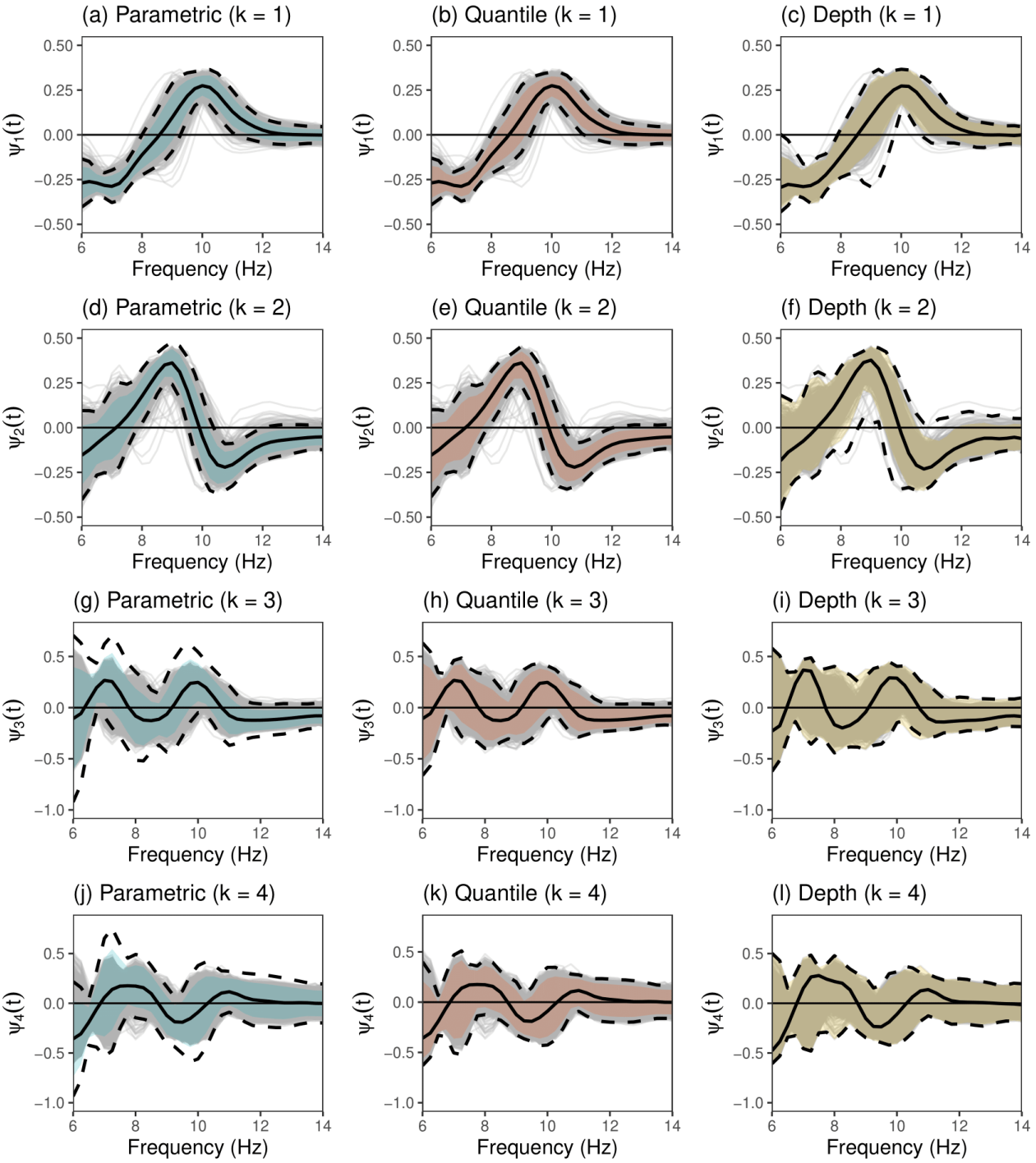

Figure S13: 95% parametric and quantile credible intervals along with 95% CPEs for the leading four eigenfunctions in our data application. The light grey solid lines represent the sample of $M = 4000$ posterior estimates. The blue, red, and yellow shaded regions represent $P^p_{.95}\{\psi_k(t)\}$, $Q^p_{.95}\{\psi_k(t)\}$, and $D_{.95}\{\psi_k(t)\}$, respectively. The black dashed lines in the left, middle and right columns represent $P^s_{.95}\{\psi_1(t)\}$, $Q^s_{.95}\{\psi_k(t)\}$, and $D^\star_{.95}\{\psi_k(t)\}$, respectively, while the estimated eigenfunctions (eigenfunction estimate and MBD median) are given in solid black.